Antonis Kokossis, Michael C. Georgiadis, Efstratios N. Pistikopoulos (Eds.)
PROCEEDINGS OF THE 33rd European Symposium on Computer Aided Process Engineering (ESCAPE33), June 18-21, 2023, Athens, Greece
 http://dx.doi.org/10.1016/B978-0-443-15274-0.50130-X

A Machine Learning-assisted Hybrid Model to Predict Ribbon Solid Fraction, Granule Size Distribution and Throughput in a Dry Granulation Process

Yan-Shu Huang,[a] David Sixon,[a] Phoebe Bailey,[a] Rexonni B. Lagare,[a] Marcial Gonzalez,[b,c] Zoltan K. Nagy,[a] Gintaras V. Reklaitis[a]

[a]*Davidson School of Chemical Engineering, Purdue University, West Lafayette, IN 47907, USA*
[b]*School of Mechanical Engineering, Purdue University, West Lafayette, IN 47907, USA*
[c]*Ray W. Herrick Laboratories, Purdue University, West Lafayette, IN 47907, USA*
huan1289@purdue.edu

Abstract

A quantitative model can play an essential role in controlling critical quality attributes of products and in designing the associated processes. One of the challenges in designing a dry granulation process is to find the optimal balance between improving powder flowability and sacrificing powder tabletability, both of which are highly affected by ribbon solid fraction and granule size distribution (GSD). This study is focused on developing a hybrid machine learning (ML)-assisted mechanistic model to predict ribbon solid fraction, GSD, and throughput for the purpose of implementing model predictive control of an integrated continuous dry granulation tableting process. It is found that the predictability of ribbon solid fraction and throughput are improved when modification is made to Johanson's model by incorporating relationships between roll compaction parameters and ribbon elastic recovery. Such relationships typically are either not considered or assumed to be a constant in the models reported in the literature. To describe the nature of the bimodal size distribution of roller compactor granules instead of only using traditional D_{10}, D_{50} and D_{90} values, the GSD is represented by a bimodal Weibull distribution with five fitting parameters. Furthermore, these five GSD parameters are predicted by ML models. The results indicate the ribbon solid fraction and screen size are the two most significant factors affecting GSD.

Keywords: dry granulation, roller compactor, machine learning, hybrid model

1. Introduction

The dry granulation process is an important route for producing a solid dosage form in the pharmaceutical industry. The roller compactor is the key unit operation in a dry granulation process. It includes two steps: (1) roll compaction in which powder blends are compressed between two counter-rotating rolls into a ribbon, and (2) milling in which these ribbons are crushed into granules. The benefits of dry granulation include improved blend uniformity and flowability by enlargement of particle size. Powder flowability plays a key role in determining the performance of the tablet manufacturing process and final drug product quality (Lagare et al., 2023). In addition, good powder flowability can reduce powder fouling and improve the on-line sensor performance, such as capacitance-

based particulate flow rate sensor (Huang et al., 2022). However, particle size over-enlargement or over-compression of powders can compromise the tabletabiltiy (Herting & Kleinebudde, 2008). Finding the optimal balance between improving powder flowability and sacrificing powder tabletability, which are highly affected by ribbon solid fraction and GSD, becomes one of the challenges in designing a dry granulation process. Therefore, quantitative models to predict ribbon solid fraction and GSD are essential to optimally operate the roller compactor.

Mechanistic models such as Johanson's model(Johanson, 1965) are typically used to describe roll compaction and further predict ribbon solid fraction. However, one of the reasons for the unsatisfactory prediction accuracy of ribbon solid fraction is due to elastic recovery, which is either not considered or assumed to be a constant in the models reported in the literature (Keizer & Kleinebudde, 2020). Population balance models (PBM) can account for the milling step and can be used to predict GSD, but it is complicated to determine the breakage function in the PBM purely based on ribbon fracture physics. Given the unknown physical nature of ribbon elastic recovery and GSD, machine learning (ML) is a preferred alternative to developing a mechanistic model. Moreover, ML and mechanistic model components can be combined into a hybrid model to maintain high physical interpretability and feasibility. Therefore, the primary objective of this work is to develop and validate a hybrid model for the purpose of implementing model predictive control of an integrated continuous dry granulation tableting process.

2.Methodology

2.1. Parameter Estimation

Given n experiments and m output variables, the procedure to estimate model parameters can be formulated as a constrained optimization problem:

$$\min_{\hat{\theta}} J = \sum_{i=1}^{n} \sum_{j=1}^{m} w_j \left(y_{j,i} - \hat{y}_{j,i}\right)^2 \tag{1}$$

$$subject\ to\ \ f\left(u, \hat{\theta}, \hat{y}\right) = 0, \qquad \hat{\theta} \in \Omega_\theta\ , \qquad \hat{y} \in \Omega_y$$

where u and y are measurements of input and output variables. $\hat{\theta}$ and $\hat{y}$ are estimated model parameters and predicted output variables, bounded in compact sets Ω_θ and Ω_y, respectively. w_j is the weighting for residual of output variable y_j.

2.2. Machine Learning

Machine learning models are common alternatives when process outputs are difficult to predict by pure mechanistic models. The multiple linear regression (MLR) model and the neural network (NN) model are employed in this study. The NN models studied consist of one hidden layer, where the hyperbolic tangent function is applied.

2.3. Experimental Methods

The material used in this study was a blend of 90 % w/w microcrystalline cellulose Avicel PH102 and 10% w/w acetaminophen. In each experiment, the Alexanderwerks WP120 roller compactor was operated for three minutes to reach a steady state, at which point samples were collected. The ribbons of interest were collected after the powders were compressed into ribbons and then broken into smaller ribbons by the flake crusher. The granulator consists of a two-stage hammer mill with two different screen sizes (screen 1 and screen 2), which produces two granule samples (granule 1 and granule 2). An in-house flowrate sensor based on a Mettler Toledo ME 4001E weighing scale was located at the roller compactor exit to capture the throughput of granules.

In order to measure the ribbon thickness, a Fisherbrand Traceable digital caliper was used to measure thirty ribbons to provide a statistically significant sample size. Geopyc 1360

pycnometer was used to measure the ribbon envelop density (ρ_e). The ribbon solid fraction (γ_R) can be computed as:

$$\gamma_R = \frac{\rho_e}{\rho_t} \tag{2}$$

where ρ_t is the powder true density, which is measured by an Accupyc II 1340 pycnometer. The GSD of granule 1 and granule 2 samples were measured by the Canty SolidSizer, which measures the size and area of each particle. In this study, the circular equivalent diameter was used and the cumulative frequency of GSD was volume-based.

3. Results and Discussion

The input and output variables of the roller compactor are shown in Figure 1. Ribbon splitting is a phenomenon causing additional uncertainty in the model accuracy and can be avoided when the roll gap and roll pressure are low.

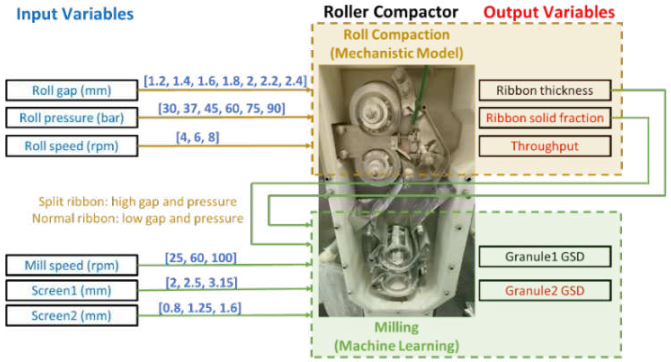

Figure 1. Roller compactor schematic.

3.1 Roll Compaction

When the materials transform from the slip condition to the non-slip condition, the stress gradients in slip region and nip region are equal. The critical angular roller position at which this occurs is known as the nip angle α and can be calculated by Johanson's model:

$$\frac{4\left(\frac{\pi}{2}-\alpha-\nu\right)\tan\delta_E}{\cot(A-\mu)-\cot(A+\mu)} - \frac{K\left(2cos\alpha-1-\frac{S}{D_R}\right)tan\alpha}{cos\alpha} = 0 \tag{3}$$

$$\text{where } A = \frac{\alpha+\nu+\frac{\pi}{2}}{2}, \qquad \nu = \frac{1}{2}\left[\pi - \sin^{-1}\left(\frac{sin\phi_w}{sin\delta_E}\right) - \phi_W\right], \qquad \mu = \frac{\pi}{4} - \frac{\delta_E}{2} \tag{4}$$

Here, δ_E is the effective angle of internal friction and ϕ_W is wall friction angle, K is compressibility factor, S is roll gap, and D_R is roll diameter.

Given roll diameter D_R and roll width W, the peak pressure (P_{max}) applied on the powders at the minimum roll gap S is computed as follows:

$$P_{max} = \frac{2P_H A_{cs}}{WD_R F} \tag{5}$$

with the force factor, F, given by

$$F = \int_0^{\alpha} \left[\frac{\frac{S}{D_R}}{\left(1-\frac{S}{D_R}-cos\theta\right)cos\theta}\right]^K cos\theta \, d\theta \tag{6}$$

where P_H is hydraulic pressure (or roll pressure) and A_{cs} is area of the compact surface. Based on a compression power law, the ribbon solid fraction at the gap γ_G can be computed as follows:

$$\gamma_G = \gamma_0 (P_{max})^{\frac{1}{K}} \tag{7}$$

where γ_0 is the pre-consolidation solid fraction. However, γ_G is not easily measured because ribbon elastic relaxation makes ribbon density decrease when ribbons are

released from the roll. Given the elastic recovery β, the ribbon solid faction γ_R is represented as follows:

$$\gamma_R = \frac{\gamma_G}{\beta} \tag{8}$$

Considering mass balance around the roll gap and roll speed N_R, the mass throughput can be calculated as follows:

$$\dot{M} = \pi D_R W S N_R \rho_t \gamma_G = \pi D_R W S N_R \rho_t \beta \gamma_R \tag{9}$$

In this work, 15 sets of training data and 4 sets of test data are used to validate and evaluate three roll compaction models. First, a data-driven MLR model is built as a benchmark. Secondly, roll compaction mechanistic models are highly sensitive to powder compressibility K and powder pre-consolidation solid fraction γ_0(Toson et al., 2019). Instead of using common regression approaches to estimate these two model parameters, this study estimates parameters in a constrained optimization framework as follows:

$$\min_{\phi_W,\, \delta_E,\, K,\, \gamma_0, \beta} J = \sum_{i=1}^{n} [W_\gamma \left(\gamma_{R,i} - \hat{\gamma}_{R,i}\right)^2 + W_M \left(\dot{M}_i - \hat{\dot{M}}_i\right)^2] \tag{10}$$

Thirdly, elastic recovery is known to be a function of roll compaction parameters instead of a constant. Under the assumption that measured elastic recovery is the ratio of measured ribbon thickness to roll gap, the predicted elastic recovery β is formulated as:

$$\beta_{Model3} = 0.96 + 0.12\frac{S}{S_0} + 0.03\frac{P_H}{P_{H0}} + 0.01\frac{N_R}{N_{R_0}} \tag{11}$$

where β_{Model3} has training error MAPE = 4.17 % and test error MAPE = 10.67%. To further improve the elastic recovery predictability, it is worth investigating ribbon splitting phenomenon and other nonlinear ML models in future studies. The prediction performances of the three roll compaction models are summarized in Table 1, which is calculated using the test sets. By incorporating the relationships between roll compaction parameters and ribbon elastic recovery, Model3 has the smallest mean absolute percentage error (MAPE) for both ribbon solid fraction and mass throughput, indicating the best model performance. The parity plot for Model3 is shown in Figure 2.

Table 1. Roll compaction model performance.

Model	MAPE(γ_R) [%]	MAPE($\dot{M}$) [%]
Model1 (MLR)	5.68	9.98
Model2 (Johanson's with constant β)	4.40	5.01
Model3 (Johanson's with $\beta = \beta_{model3}$)	2.86	4.61

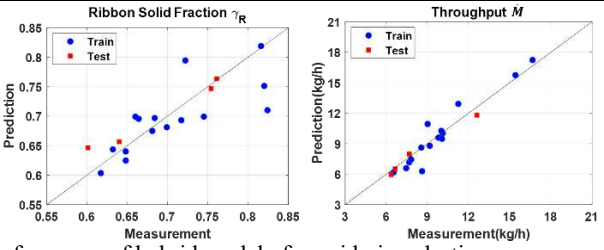

Figure 2. Performance of hybrid model of considering elastic recovery model (Model3).

3.2 Milling

The hammer milling step commonly produces granules with a bimodal size distribution, which is not adequately described by only using D_{10}, D_{50} and D_{90} values. Therefore, the entire cumulative size distribution $D_5, D_{10}, \ldots, D_{95}$ measured with the Canty SolidSizer is represented by a bimodal GSD, which can be characterized by a cumulative bimodal Weibull distribution $Q_3(x)$:

$$Q_3(x) = a\left(1 - e^{-\left(\frac{x}{p_1}\right)^{m_1}}\right) + (1-a)\left(1 - e^{-\left(\frac{x}{p_2}\right)^{m_2}}\right) \tag{12}$$

where a is the weighting of the two modes, p_1 and p_2 are the size parameters of the small mode and large mode, respectively, whereas $m_1$and m_2 represent the shape parameters of the associated modes. Utilizing these statistical model parameters provides a more interpretable approach to describing GSD and reduces the GSD parameter set from 19 to 5. The bimodal Weibull distribution parameters can be computed by solving an optimization problem:

$$\min_{a,\,p_1,\,p_2,m_1,m_2} J = \sum_{i=5,10\ldots}^{95}\left(\frac{i}{100} - Q_3(D_i)\right)^2 \tag{13}$$

$$subject\ to\ 0 \le a \le 1, \quad 0 < p_1 < p_2, \quad 1 < m_1,\ m_2$$

To link the roll compaction and milling process, the ribbon solid fraction γ_R and ribbon thickness ($Rtck$) serve as inputs of the milling model. In addition, milling speed ($Mill$) and screen size(s) are also used to predict the GSD described by five bi-modal Weibull fitting parameters. The sensitivity analysis of both granule 1 and granule 2 are shown in Figure 3. The sensitivity analysis was determined by the MLR model coefficient, where inputs and outputs were both rescaled by dividing the minimum values. In terms of weighting a, ribbon solid fraction of granule 1 is dominated by ribbon solid fraction while that of granule 2 is more sensitive to screen size. For both granule 1 and granule 2, the size parameter p_1 is highly related to ribbon solid fraction. On the other hand, p_2 is dominated by screen size given that screen size determines the upper boundary of the particle size. Shape parameter m_1 is less sensitive to all process inputs compared to the shape parameter m_2, which is highly impacted by the solid ribbon fraction.

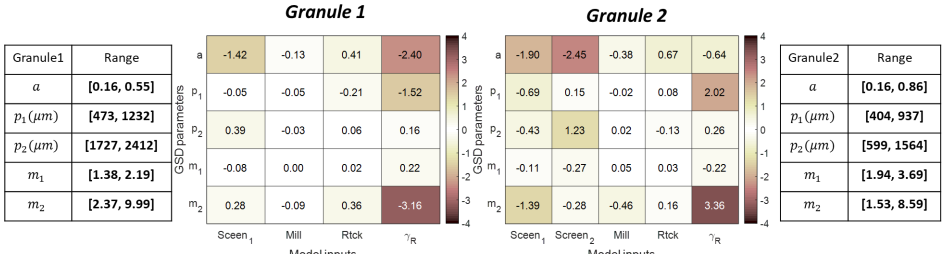

Granule1	Range
a	[0.16, 0.55]
$p_1(\mu m)$	[473, 1232]
$p_2(\mu m)$	[1727, 2412]
m_1	[1.38, 2.19]
m_2	[2.37, 9.99]

	Sceen1	Mill	Rtck	γ_R
a	-1.42	-0.13	0.41	-2.40
p_1	-0.05	-0.05	-0.21	-1.52
p_2	0.39	-0.03	0.06	0.16
m_1	-0.08	0.00	0.02	0.22
m_2	0.28	-0.09	0.36	-3.16

	Sceen1	Screen2	Mill	Rtck	γ_R
a	-1.90	-2.45	-0.38	0.67	-0.64
p_1	-0.69	0.15	-0.02	0.08	2.02
p_2	-0.43	1.23	0.02	-0.13	0.26
m_1	-0.11	-0.27	0.05	0.03	-0.22
m_2	-1.39	-0.28	-0.46	0.16	3.36

Granule2	Range
a	[0.16, 0.86]
$p_1(\mu m)$	[404, 937]
$p_2(\mu m)$	[599, 1564]
m_1	[1.94, 3.69]
m_2	[1.53, 8.59]

Input	Screen1 (mm)	Screen2 (mm)	Mill (rpm)	Rtck (mm)	γ_R
Range	[2, 3.15]	[0.8, 1.6]	[25, 100]	[1.67, 3.23]	[0.62, 0.79]

Figure 3. Sensitivity analysis of the milling process.

To evaluate the performance of the milling models, the MAPE of GSD is utilized and can be computed as:

$$MAPE = \sum_{i=1}^{n}\sum_{p=5,10,\ldots}^{95}\left|\frac{D_{p,i}^{pred} - D_{p,i}}{D_{p,i}}\right| \times 100\% \tag{14}$$

The evaluation of the milling models is summarized in Table 2, which is based on 20 training sets and 6 test sets. MLR and NN models are used to predict GSD. The NN models have two neurons in the hidden layer. While increasing the number of neurons can readily make the training error of the NN model smaller than that of the MLR model, the test error can become much worse due to overfitting. The NN model generally can handle nonlinearity better than the MLR model, but some constraints might be hard to enforce, e.g., predicted shape parameters m_1 and m_2 might be less than 1 in the test sets. Figure 4 demonstrates the predictability of the granule 2 GSD by using the MLR or NN models based on six test sets. It is worth noting that there exists a significant mismatch between measurement and NN predictions in Exp 6, but the NN model prediction seems more reasonable considering that screen 2 is 1.25 mm and Exp 6 has a smaller ribbon solid fraction compared to Exp 3, which should result in a smaller GSD. In summary, the

hybrid model successfully predicts GSD, and further investigation of different ML models might be useful to enhance the model performance.

Table 2 Milling model performance.

Model	Granule1		Granule2	
	$MAPE_{train}$ (%)	$MAPE_{test}$ (%)	$MAPE_{train}$ (%)	$MAPE_{test}$ (%)
MLR	9.79	11.21	10.89	8.95
NN	9.66	12.20	13.03	8.37

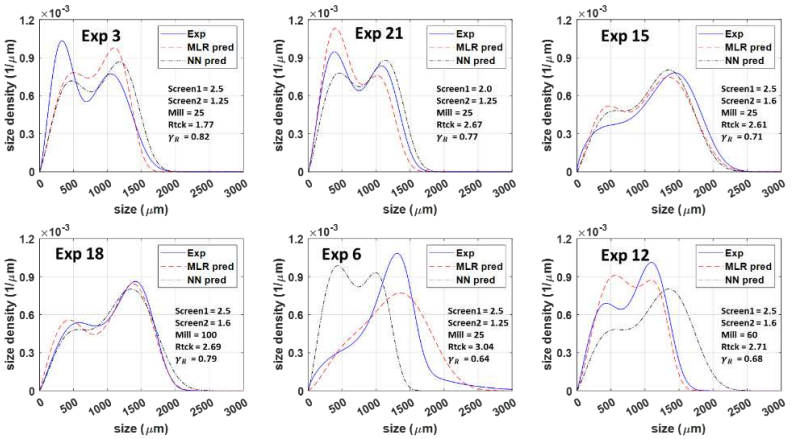

Figure 4. Model prefomance of granule2 based on test sets.

4. Conclusion

A hybrid model for the roller compactor is proposed that demonstrates satisfactory predictability of ribbon solid fraction, throughput, and GSD. To further improve the model performance, investigation on ribbon elastic recovery and splitting phenomenon and incorporation constraints into ML model could be important. Future work will include relating ribbon solid fraction and GSD to the tablet properties and implementing model predictive control of the integrated dry granulation tableting process.

Acknowledgement

This work was supported by the National Science Foundation under Grant No. 2140452 - CMMI-EPSRC: Right First Time Manufacture of Pharmaceuticals (RiFTMaP)

References

Herting, M. G., & Kleinebudde, P. (2008). Studies on the reduction of tensile strength of tablets after roll compaction/dry granulation. *European Journal of Pharmaceutics and Biopharmaceutics*, *70*(1), 372–379.

Huang, Y. -S., Medina-González, S., Straiton, B., Keller, J., Marashdeh, Q., Gonzalez, M., Nagy, Z., & Reklaitis, G. v. (2022). Real-Time Monitoring of Powder Mass Flowrates for Plant-Wide Control of a Continuous Direct Compaction Tablet Manufacturing Process. *Journal of Pharmaceutical Sciences*, *111*(1), 69–81.

Johanson, J. R. (1965). *A Rolling Theory for Granular Solids Theory and Method of Calculation*.

Keizer, H. L., & Kleinebudde, P. (2020). Elastic recovery in roll compaction simulation. *International Journal of Pharmaceutics*, *573*.

Lagare, R. B., Huang, Y.-S., Bush, C. O.-J., Young, K. L., Rosario, A. C. A., Gonzalez, M., Mort, P., Nagy, Z. K., & Reklaitis, G. v. (2023). Developing a Virtual Flowability Sensor for Monitoring a Pharmaceutical Dry Granulation Line. *Journal of Pharmaceutical Sciences*.

Toson, P., Lopes, D. G., Paus, R., Kumar, A., Geens, J., Stibale, S., Quodbach, J., Kleinebudde, P., Hsiao, W. K., & Khinast, J. (2019). Model-based approach to the design of pharmaceutical roller-compaction processes. *International Journal of Pharmaceutics: X*, *1*, 100005.